Electron velocity distributions during beam–plasma interaction

Q. M. Lu[a] and S. Wang
School of Earth and Space Sciences, University of Science and Technology of China, Hefei, Anhui 230026, People's Republic of China

(Received 15 August 2003; accepted 14 October 2003)

It is well known that low-frequency Alfvén waves can be excited due to an ion/ion instability when a tenuous ion beam streams through a background plasma along a magnetic field. In this article, using a one-dimensional particle-in-cell code, the consequence of this beam–plasma interaction process is investigated. Emphasis is placed on the nonlinear effects of enhanced Alfvén waves on beam electrons. In the simulation, the speed between the beam plasma and ambient plasma is considered to be $10\,V_A$ (where V_A is the Alfvén speed), the ratio of beam–plasma density to background plasma density is $n_b/n_0=0.006$ (n_b and n_0 are the beam and total plasma densities). For the case $\beta_i=4\times10^{-4}$ (β_i being the ratio of kinetic pressure of the ions to magnetic pressure), the Alfvén waves begin to grow exponentially at about $t=32\,\Omega_i^{-1}$, and they saturate at about $t=88\,\Omega_i^{-1}$. The excited waves are nearly monochromatic, which satisfies the resonant condition, and the perpendicular velocity (the velocity component whose direction is perpendicular to the ambient magnetic field) distribution of the beam electrons peaks away from its origin with a maximum radius about $2.5\,V_A$ at the saturation stage. Then, the amplitude of the excited waves decreases and the higher-frequency waves are also excited. A quasi-equilibrium stage is reached at about $t=100\,\Omega_i^{-1}$, and the radius of the ring in the perpendicular velocity distribution is about $0.7\,V_A$. For the case $\beta_i=0.04$, the situation is similar except that the radius of the ring in the perpendicular velocity distribution of the beam electrons is smaller, and the ring almost disappears at the quasi-equilibrium stage. Another point is that both the beam and background electrons can be heated by the excited Alfvén waves. The heating effect is more significant for the beam electrons than the background electrons, and their final thermal speeds are anticorrelated with the parameter β_i.
 [DOI: 10.1063/1.1631288]

I. INTRODUCTION

It is well known that two interpenetrating plasmas moving relatively along an ambient magnetic field can lead to plasma instabilities, enhanced field fluctuations, and wave–particle scattering. Among these, electromagnetic ion/ion instabilities have attracted much theoretical interest due to many relevant applications in space physics research, such as the study of the Earth's magnetotail,[1,2] bow shock,[3–5] and solar wind.[6–8] Not only can ion beam instabilities explain many commonly observed wave activities, but also, in some cases, the instability can play pivotal roles that lead to essential consequences. An outstanding example is that the ion/ion beam instability can lead to energy and momentum transfer between two plasmas in the absence of Coulomb collisions. It is by this process that the solar wind can pick up newly created ions of interstellar,[9–11] solar,[12,13] and cometary origins.[14–18]

One of the reasons, that has made the electromagnetic ion-beam instability very important is that under certain conditions the ion beam can excite ultralow-frequency hydromagnetic waves, such as Alfvén waves, which can in turn result in pitch–angle scattering, a process which can efficiently modify and isotropize the ion-beam distribution. Moreover, it was also found in a recent study that the enhanced Alfvén waves can also lead to the heating of the ambient plasma.[19] Such a finding was unexpected because conventional wisdom based on linear theory seems to predict that Alfvén waves can only interact with beam ions but not with the ambient plasma. The reason is that in linear theory, wave–ion interactions rely on the resonant condition, which cannot be satisfied by the thermal ions. However, recent theoretical studies by Li *et al.*,[19] Wu *et al.*,[20] and Chen *et al.*[21] have convinced us that nonlinear interactions do not require cyclotron resonance. Enhanced Alfvén waves can directly interact with low-energy ions.

Inspired by this finding, we question whether the enhanced Alfvén waves could nonlinearly interact with fast electrons. According to linear theory, an electron beam cannot excite Alfvén waves just because no cyclotron resonant interaction between electrons and Alfvén waves is possible. The emerging issue is whether interactions via nonlinear processes are possible.

The reason why we are interested in beam electron distribution function will be briefly explained. It is well known that in plasma physics literature, we usually model the distribution function of an electron beam by a displaced Maxwellian distribution function, which represents a standard approach. However, it may or may not be the best way to describe the realistic situation, particularly in the solar–terrestrial environment where enhanced Alfvénic turbulence is pervasive. In some cases, both energetic protons and elec-

[a]Electronic mail: qmlu@ustc.edu.cn

trons may be produced at the same time, so that the beaming particles actually involve both species. The protons can excite Alfvén waves if the beam velocity is sufficiently higher than the Alfvén speed, although the streaming electrons cannot. We are interested in whether the ensuing Alfvénic turbulence can then modify the beam electrons via nonlinear interactions. To investigate this issue is the principal purpose of the present study.

In literature, all previous studies of the ion-beam instability mentioned earlier have made use of hybrid-code simulations. Evidently, in the present case, a full particle code is necessary because we are ultimately interested in the distribution function of the streaming electrons. The organization of this article is as follows. The simulation model is described in Sec. II. The one-dimensional (1D) particle-in-cell (PIC) simulation results and discussion are presented in Sec. III, and conclusions are given in Sec. IV.

II. SIMULATION MODEL

A 1D PIC code based on the explicit algorithm is used in this article. In PIC simulations, the electromagnetic fields are defined in grids, and they are updated by the Maxwell equations; while the ions and electrons are taken as discrete particles, they can be anywhere in the simulation domain and advance in the electromagnetic fields according to their equations of motion.[22,23] Although relativistic effects are included in the original code, they have no impact on the results in the present study. The 1D simulations allow spatial variations only in the x direction, but include the full three-dimensional velocities and electromagnetic fields, and the ambient magnetic field $\mathbf{B}_0$ is parallel to the x axis.

Initially, the beam and background particles are distributed uniformly in the simulation domain, where both the beam and background particles consist of ions and electrons with same number density. The beam ions and electrons flow in the $+x$ direction with the same bulk velocity $V_b = 10\ V_A$ relative to the background plasma. Initially, the beam ions are assumed to possess the following distributions:

$$f \sim \exp\left(- \frac{(u_\parallel - u_b)^2}{\Delta^2} \right) \exp\left(- \frac{(u_\perp - u_s)^2}{\alpha^2} \right),$$

where $u = \gamma v$ (γ is the relativistic factor, and v is the particle velocity) is the momentum per unit mass, subscripts $\parallel$ and $\perp$ refer to the directions parallel and perpendicular to the ambient magnetic field $\mathbf{B}_0$, respectively, and $u_s = 1.7\ V_A$. The distributions of the background ions and electrons are assumed to be Maxwellian, and the distribution of the beam electrons is a displaced Maxwellian distribution. It is considered that the temperature of the ions is four times that of the electrons. The ratio of the ion to electron mass is set to be $m_i/m_e = 400$ in our simulation, where the subscripts i and e denote the quantities associated with ions and electrons, respectively. The system length used in the present simulation is $L_x = 256\ c/\omega_{\rm pi}$, where c is the speed of light (here, we assume $c = 40\ V_A$), $\omega_{\rm pi} = (n_0 e^2/m_i \varepsilon_0)^{1/2}$ is the ion–plasma frequency, and $c/\omega_{\rm pi}$ is the ion inertial length. The grid cell is $\Delta x = 2.0 c/\omega_{\rm pi}$, and the time step is $\Delta t = 0.0005\ \Omega_i^{-1}$, where $\Omega_i = eB_0/m_i$ is the ion–gyro frequency. We use 400 super-particles per cell for each species, and the beam density is $n_b/n_0 = 0.006$. Periodic boundary conditions are employed in our simulation.

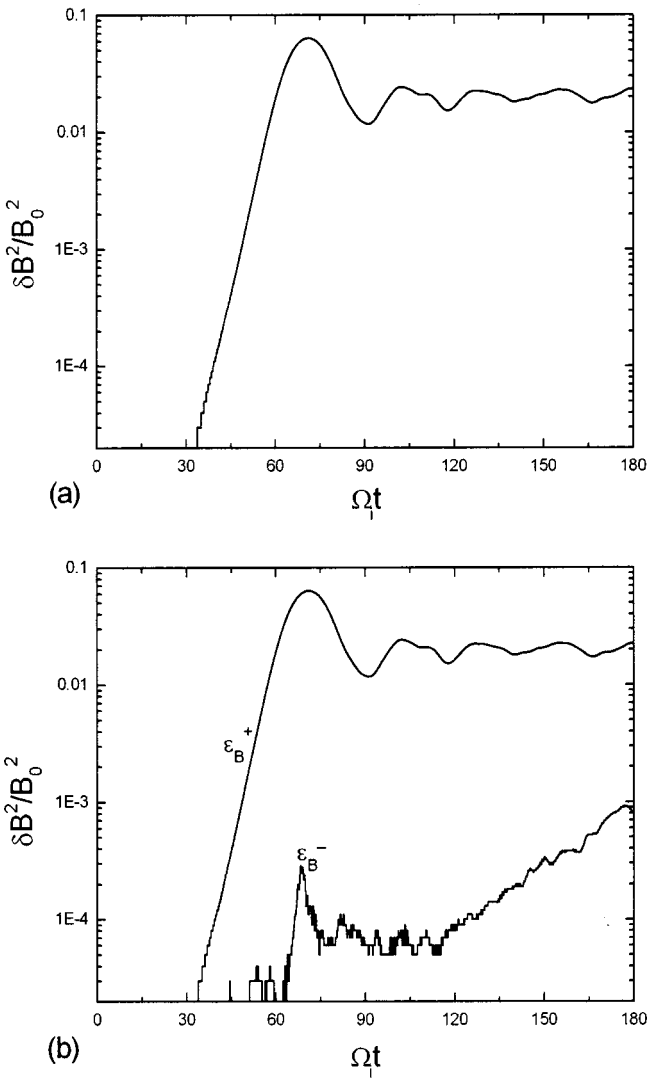

FIG. 1. The time evolutions of magnetic field energy in logarithmic scale, the parameters are $n_b/n_0 = 0.006$ and $\beta_i = 4 \times 10^{-4}$. (a) Total wave energy (ε_B). (b) Energy of waves with positive helicity (ε_B^+) and negative helicity (ε_B^-).

Normalization of physical quantities is described as follows. The length is expressed in units of $c/\omega_{\rm pi}$, and the time is normalized to Ω_i^{-1}. The velocity is expressed in units of V_A. The magnetic and electric fields are expressed in units of B_0 and $V_A B_0$, respectively.

III. SIMULATION RESULTS

In the first case, we set the plasma $\beta_i = 4 \times 10^{-4}$. Previous studies reported in literature find that waves due to the resonant beam instability excite waves with positive helicity, (a right-hand side mode that propagates to the $+x$ direction) whereas the nonresonant instability excites waves with negative helicity (a right-hand side mode that propagates to the $-x$ direction). Taking advantage of this fact, we can study the excitation process by separating the wave fields into positive and negative helical parts.[24,25] Figure 1 shows the time

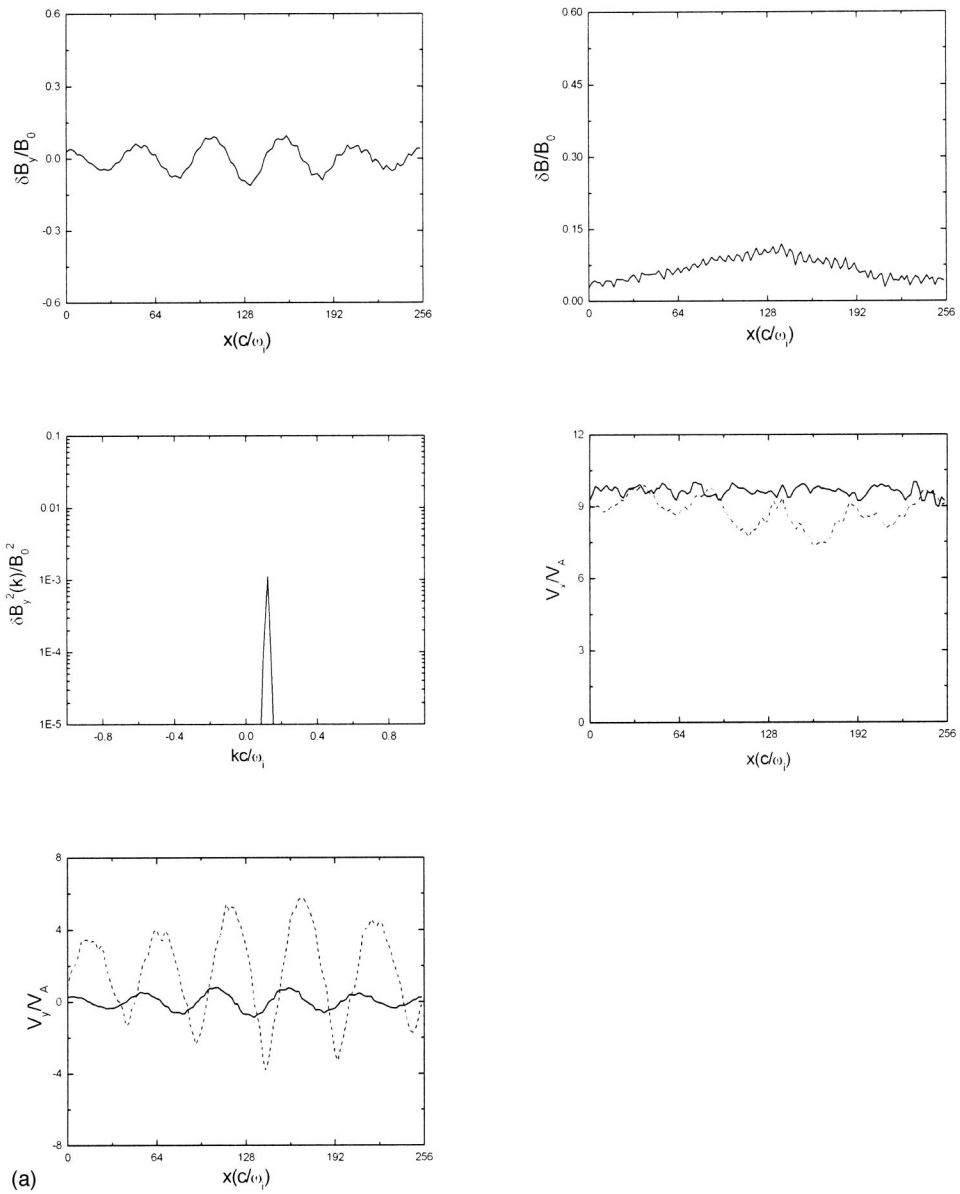

FIG. 2. The field quantities δB_y, $\delta B=\sqrt{\delta B_y^2+\delta B_z^2}$, the Fourier power spectrum $\delta B_y^2(k)$, the bulk velocity of beam ions (dashed line) and electrons (solid line) V_x, V_y at (a) $t=52\,\Omega_i^{-1}$, (b) $68\,\Omega_i^{-1}$, (c) $88\,\Omega_i^{-1}$, and (d) $172\,\Omega_i^{-1}$ which correspond to initial growth (prediction from the linear theory), saturation, postsaturation and quasi-equilibrium stages, respectively. The parameters are $n_b/n_0=0.006$ and $\beta_i=4\times10^{-4}$.

evolution of $\varepsilon_B=\delta B^2/B_0^2$, the total magnetic field energy, ε_B^+, the magnetic field energy of the positive waves, and ε_B^-, the magnetic field energy of the negative waves in logarithmic scales. Obviously, the right-hand side resonant instability, which corresponds to Alfvén waves, dominates and, thus, the nonresonant instability is negligible. This conclusion is consistent with the previous discussions and hybrid simulations.[26,27] From about $t=32\,\Omega_i^{-1}$, the resonant wave begins to grow in time, and it saturates at about $t=68\,\Omega_i^{-1}$. It reaches a quasi-equilibrium stage at about $100\,\Omega_i^{-1}$.

Figure 2 describes the field quantities δB_y, $\delta B=\sqrt{\delta B_y^2+\delta B_z^2}$, the Fourier power spectrum $\delta B_y^2(k)$, the bulk velocity of beam ions and electrons V_x, V_y at $t=52\,\Omega_i^{-1}$, $68\,\Omega_i^{-1}$, $88\,\Omega_i^{-1}$, and $172\,\Omega_i^{-1}$ which correspond to initial growth (prediction from the linear theory), saturation, postsaturation and quasi-equilibrium stages, respectively. In this Fourier power spectrum $\delta B_y^2(k)$, the positive sign "+" of k means that excited waves have positive wave numbers, which are the right-hand side resonant modes propagating to the $+x$ direction; while the negative sign "−" of k corresponds to the right-hand side nonresonant modes propagating to the $-x$ direction, which have the negative wave numbers. The characteristics of the four different stages are described as follows.

At the linear growth stage, the right-hand side mode has a nearly monochromatic wave spectrum, and the wave number is about $0.12\,\omega_i/c$. It satisfies the gyro resonant condition involving ions and Alfvén waves:

$$\omega+\Omega_i-k\nu_{\parallel}\approx 0, \tag{1}$$

where $\omega=kV_A$ is the Alfvén wave dispersion relation, $\nu_{\parallel}$ is

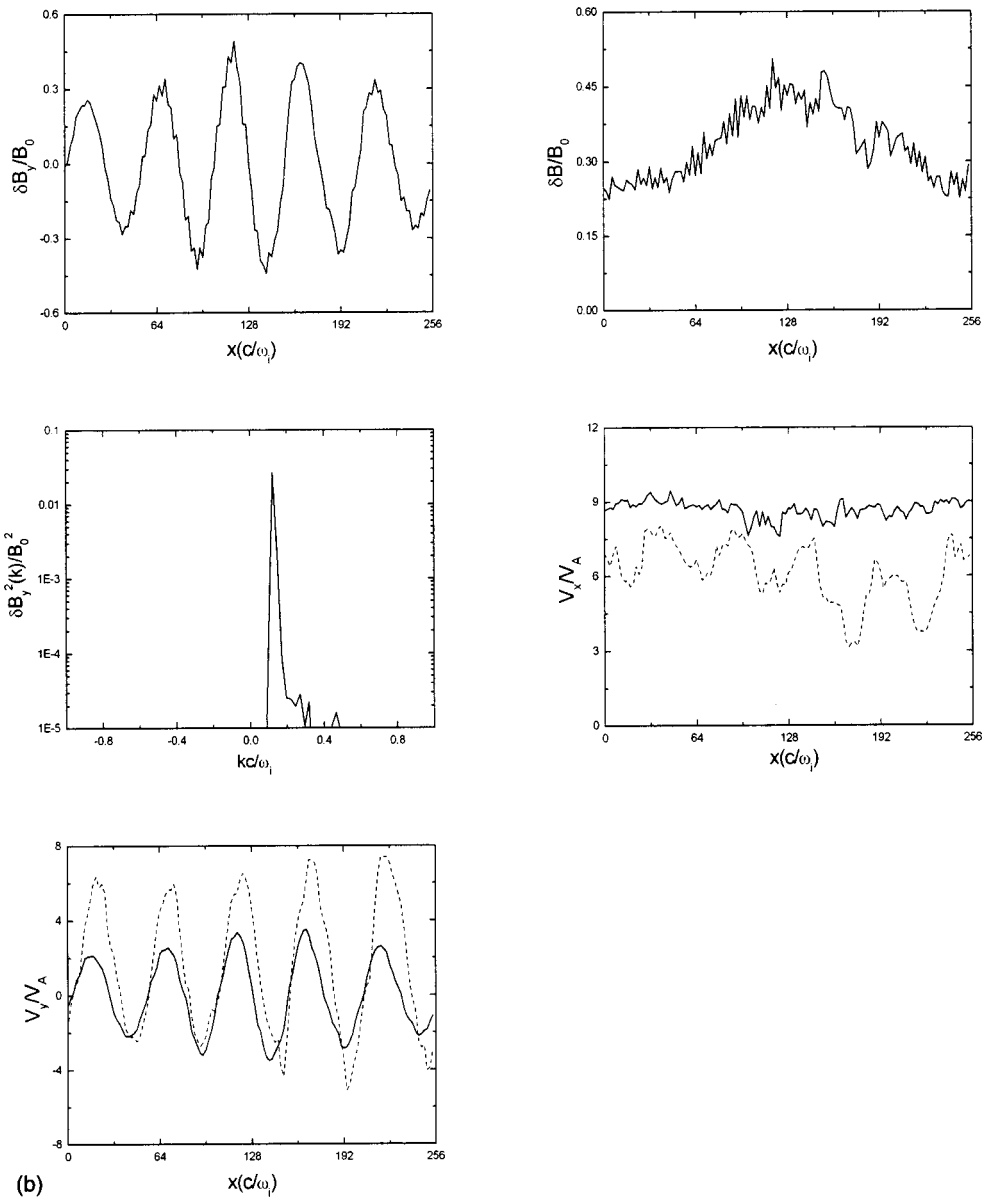

FIG. 2. (*Continued*.)

the velocity of beam ions which interact with the Alfvén waves. At this stage, we can use the bulk velocity of the beam plasma $V_b = 10\,V_A$ to stand for $\nu_\parallel$, so we get $k = 0.11\,\omega_i/c$. Magnetic pulsations are formed at about $x = 128c/\omega_i$, which steepen progressively. The magnetic pulsation traps the beam ions and electrons via gyro-phase bunching. Thus, the bulk velocity of the beam ions and electrons in the $+x$ direction decreases at the position of the magnetic pulsation, and the influence of the magnetic pulsation decelerates the beam ions more efficiently than the beam electrons. Figure 2 also shows a nearly positive correlation between the bulk velocity of the beam ions and electrons in the y direction and δB_y, but the amplitude of the bulk velocity of the beam ions is larger than that of the beam electrons. It is same for the bulk velocity of the beam ions and electrons in the z direction and δB_z (not shown).

At the saturation stage, the situation is similar to the linear growth stage, except that the amplitude of the magnetic field and the beam plasma bulk velocity are larger. The magnetic pulsations are obvious, and they propagate to the $+x$ direction with a speed about $1.0\,V_A$. More beam ions are trapped by the magnetic pulsation than at the linear growth stage. Thus, the beam ion velocity parallel to the ambient magnetic field $\nu_\parallel$ is dispersed. According to Eq. (1), waves with higher wave numbers can be excited. The result is that the wave spectrum is broadened.

At the postsaturation stage, the magnetic pulsations split, and an increasing number of spiky magnetic pulsations emerge, and, moreover, the widths and amplitudes of the pulsations vary from place to place. The beam ions are still trapped by the magnetic pulsations, but the beam electrons cannot be trapped. The positive correlation between the bulk velocity of the beam electrons in the y direction and δB_y can still be found, but the bulk velocity of the beam ions begins to deviate this positive correlation. In summary, more resonant waves with higher wave numbers, as well as the non-

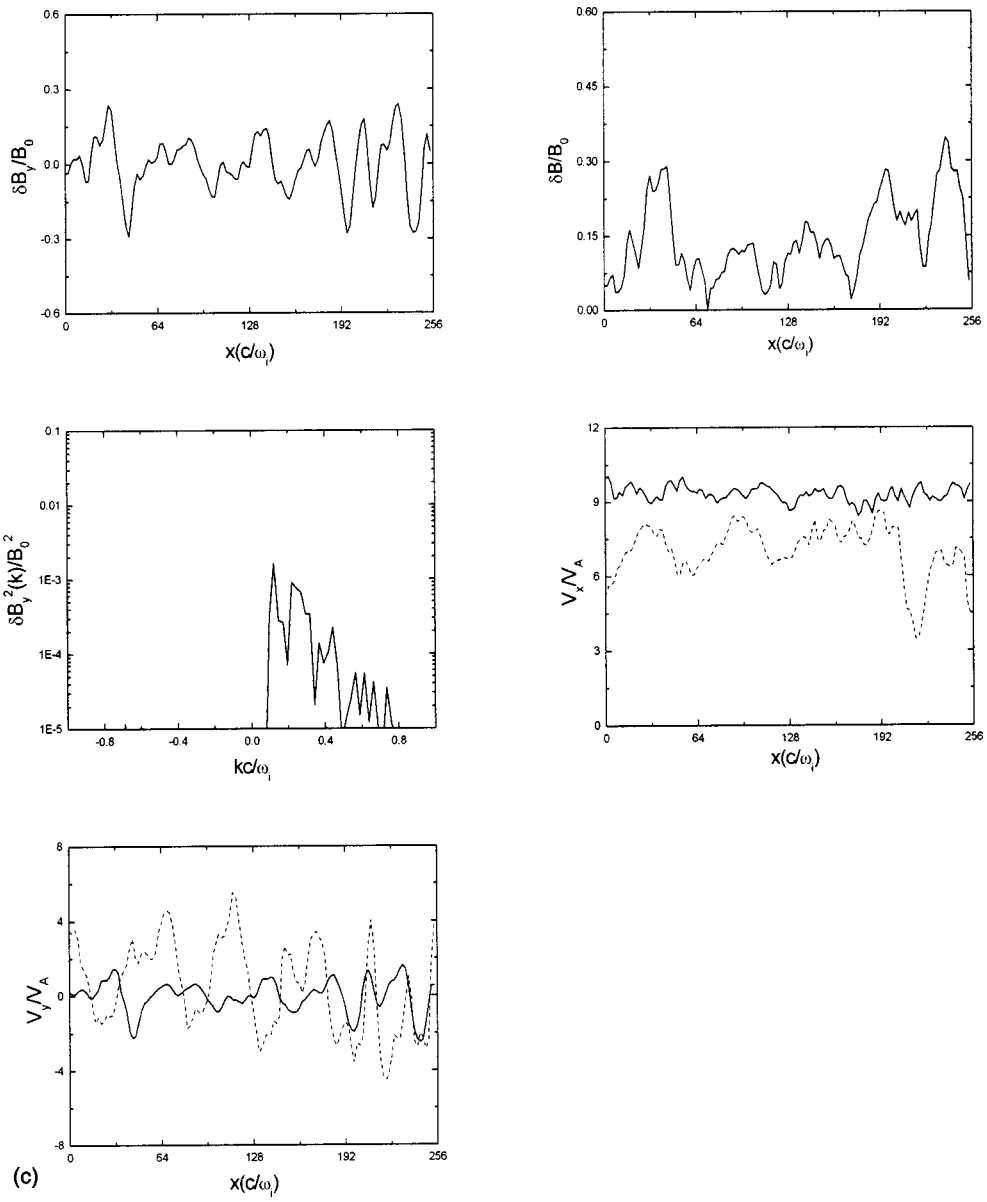

FIG. 2. (*Continued.*)

resonant waves, are excited at this stage, although the level of the nonresonant waves is negligible.

At the quasi-equilibrium stage, the wave spectrum of the excited mode becomes very broad, and more magnetic energy is transferred to higher wave number modes. The characteristic scale size of the magnetic pulsation λ is roughly equal to the wavelength of the excited resonant waves. The bulk velocity of beam ions is about $5.0\,V_A$, while the bulk velocity of the beam electrons remains almost unchanged in the same spatial region, which is about $8.2\,V_A$. A positive correlation between the bulk velocity of the beam ions and electrons in the y direction and δB_y can be found.

Figure 3 shows the reduced velocity distributions of the beam electrons $f(u_\parallel)$ and $f(u_\perp)$ at $t=52\,\Omega_i^{-1}$, $68\,\Omega_i^{-1}$, $88\,\Omega_i^{-1}$, and $172\,\Omega_i^{-1}$. Initially, the reduced velocity distributions of the beam electrons $f(u_\parallel)$ and $f(u_\perp)$ are Gaussian distributions. Later on, the distribution $f(u_\parallel)$ evolves only slightly from the initial Gaussian distribution with a small increase of the momentum dispersion due to the effect of the enhanced Alfvén waves until the quasi-equilibrium stage. On the other hand, the situation for the reduced velocity distribution of the beam electrons $f(u_\perp)$ is different. The Alfvén waves can scatter it into a ring distribution such that $\partial f(u_\perp)/\partial u_\perp > 0$ exists near $u_\perp = 0$. The ring distribution begins to form at about $t=48\,\Omega_i^{-1}$, and its radius is positively correlated with the fluctuation level of the excited Alfvén waves. The radius is about $2.5\,V_A$ at $68\,\Omega_i^{-1}$ and $0.2\,V_A$ at $88\,\Omega_i^{-1}$. In the quasi-equilibrium stage, the ring distribution persists, and the radius is about $0.7\,V_A$ at $t=172\,\Omega_i^{-1}$. The reduced distribution can be modeled by a function $f(u_\perp) \sim \exp[-(u_\perp - u_s)^2/\alpha^2]$ as considered in Wu *et al.*[28]

Previous hybrid simulations show that the background ions, as well as the beam ions, can be heated by the excited Alfvén waves with a high turbulence level,[19] however, whether the beam and background electrons can be heated by

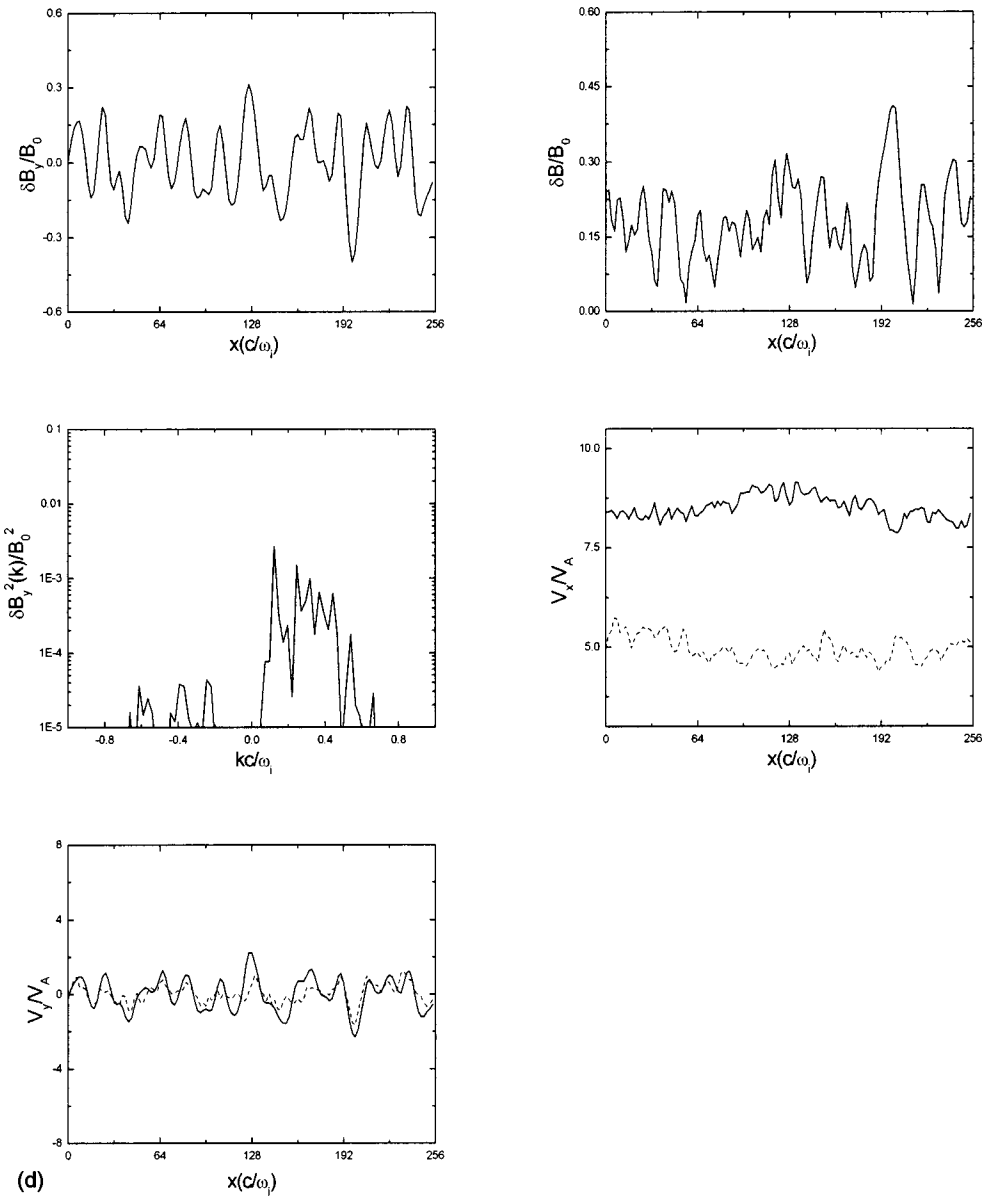

FIG. 2. (*Continued.*)

the excited Alfvén waves has never been studied. Figure 4 presents the thermal speed of the beam and background electrons as a function of time, both the beam and background electrons begin to be rapidly heated at about $t=50\,\Omega_i^{-1}$, where the turbulence level of the excited Alfvén waves is reasonably high, and the waves heat the beam electrons more effectively than the background electrons. For the beam electrons, the thermal speed in the direction perpendicular to the background magnetic field is positively correlated with the turbulence level, and it is about 11 and 6 times of its initial value at the saturation and quasi-equilibrium stages, while in the direction parallel to the background magnetic fields, the corresponding values are about 6 and 10 at the saturation and quasi-equilibrium stages. For the background electrons, although the situation is similar to the beam electrons, the heat effect by the excited Alfvén waves is less significant, at the quasi-equilibrium stage, the thermal speed is about 5.2 and 1.6 times of its initial value in the direction parallel and perpendicular to the background magnetic field, respectively. At the final phase, the velocity distribution of the background electrons is still a nearly Maxwellian distribution. One thing we need to know is that part of the heat of both the beam and background electrons in the direction parallel to the background magnetic field is attributed to the effect of charge separation between the electrons and ions, and this effect leads to the heat process for the beam electrons in the direction parallel to the background magnetic field at about $t=5\,\Omega_i^{-1}$.

In the second case, we designate $\beta_i=0.04$. Figure 5 describes the time evolution of $\varepsilon_B=\delta B^2/B_0^2$, and it is almost the same as the case $\beta_i=4\times10^{-4}$. Actually, other physical values are also similar to the case $\beta_i=4\times10^{-4}$ except the perpendicular velocity distribution of the beam electrons. Figure 6 shows the reduced perpendicular velocity distributions of the beam electrons $f(u_\perp)$ at $t=56\,\Omega_i^{-1}$, $68\,\Omega_i^{-1}$,

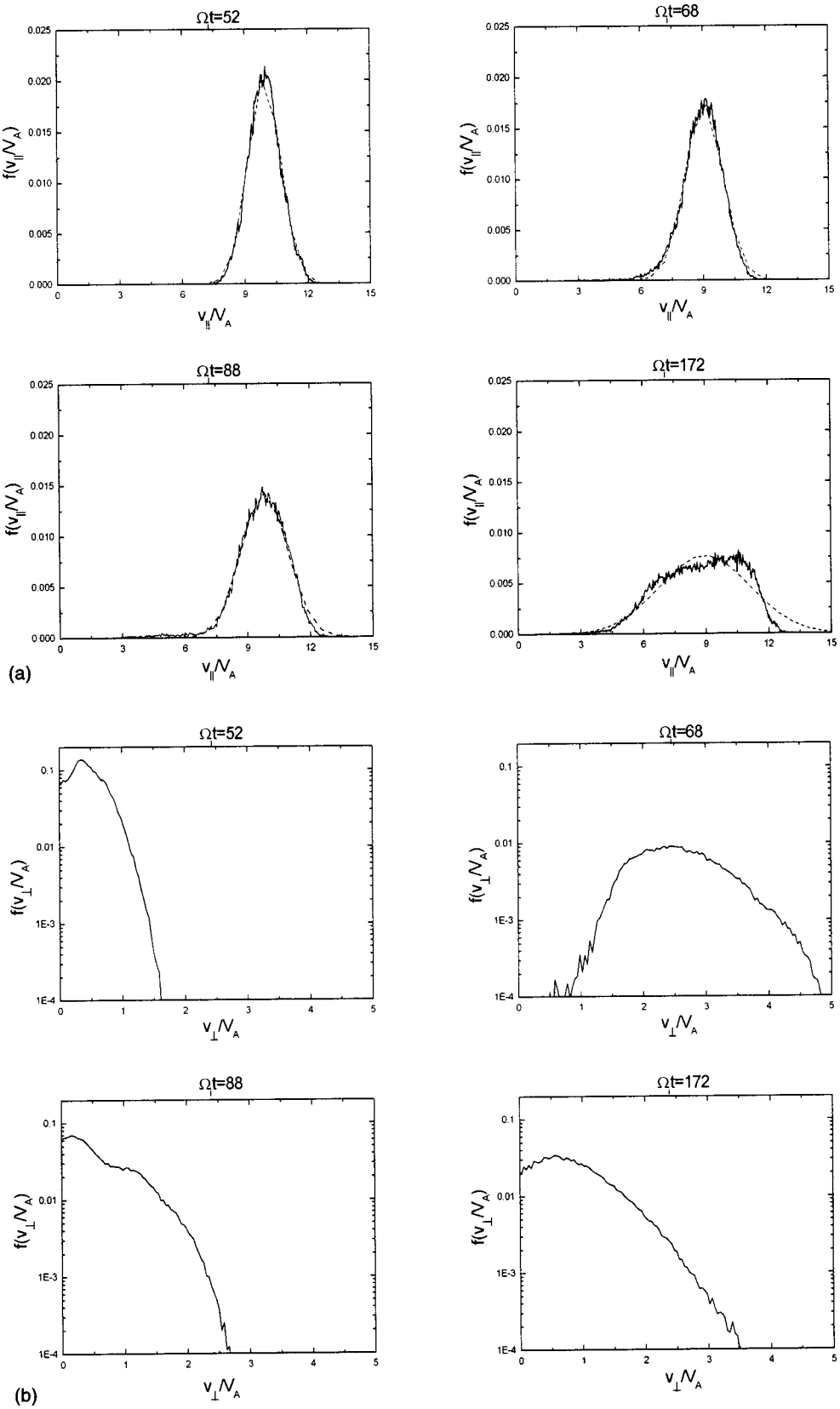

FIG. 3. The reduced velocity distributions of the beam electrons at different times $t=52\,\Omega_i^{-1}$, $68\,\Omega_i^{-1}$, $88\,\Omega_i^{-1}$, and $172\,\Omega_i^{-1}$, the parameters are $n_b/n_0=0.006$, $\beta_i=4\times10^{-4}$. (a) The reduced velocity distribution in the direction parallel to the ambient magnetic field $f(u_\parallel)$, the dashed line denotes the fitted Gaussian distribution. (b) The reduced velocity distribution in the direction perpendicular to the ambient magnetic field $f(u_\perp)$. Subscripts $\parallel$ and $\perp$ denote the directions parallel and perpendicular to the ambient magnetic field.

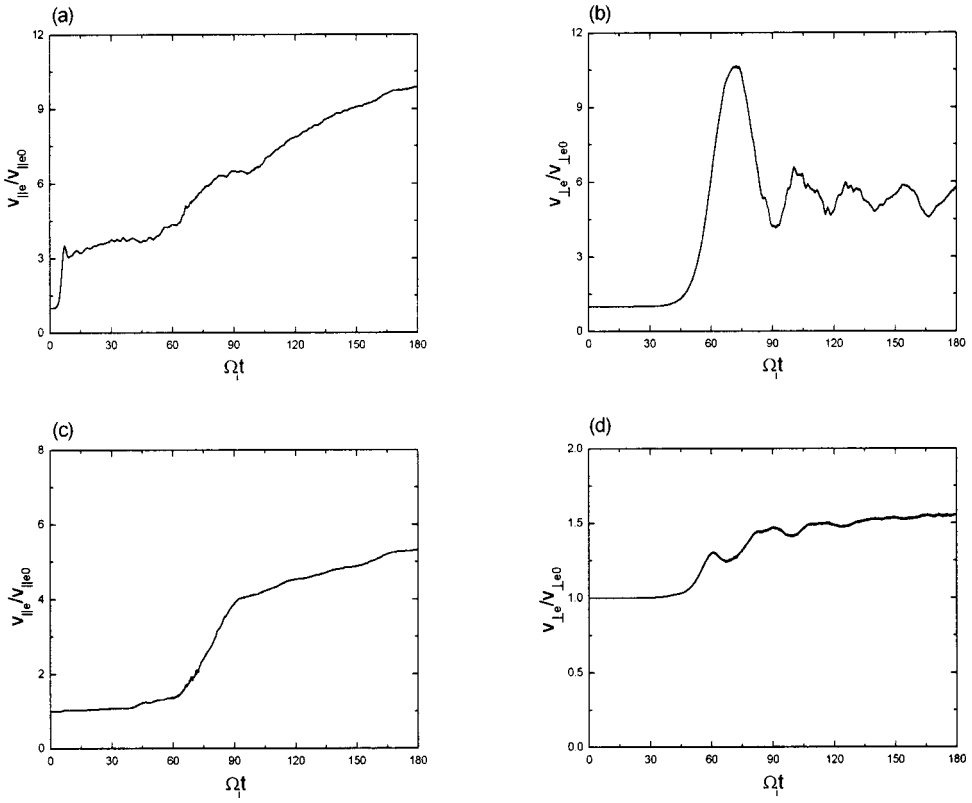

FIG. 4. The thermal speed of the beam and background electrons as a function of time, the parameters are $n_b/n_0=0.006$ and $\beta_i=4\times10^{-4}$. (a) The thermal speed of beam electrons in the direction parallel to the background magnetic field. (b) The thermal speed of beam electrons in the direction perpendicular to the background magnetic field. (c) The thermal speed of background electrons in the direction parallel to the background magnetic field. (d) The thermal speed of beam electrons in the direction perpendicular to the background magnetic field. $\nu_{\|e0}$ and $\nu_{\perp e0}$ denote the initial electron thermal speed in the direction parallel and perpendicular background magnetic field.

$76\,\Omega_i^{-1}$, and $172\,\Omega_i^{-1}$, which correspond to initial growth, saturation, postsaturation and quasi-equilibrium phases, respectively. The ring distribution of the beam electrons only appears near the saturation phase and, in other phases, the ring distribution is almost indistinguishable. Even if we increase β_i, the ring distribution of the beam electrons will also disappear at the saturation phase when $\beta_i \geqslant 0.2$. Figure 7 presents the thermal speed of the beam and background electrons as a function of time, although the excited Alfvén waves can heat the beam and background electrons, but it is much less effective than that of the $\beta_i=4\times10^{-4}$ case, the final thermal speeds of beam electrons are 1.25 and 1.50 of their initial values in the direction parallel and perpendicular to the background magnetic field, while the corresponding values are only about 1.05 and 1.01 for the background electrons that are insignificant.

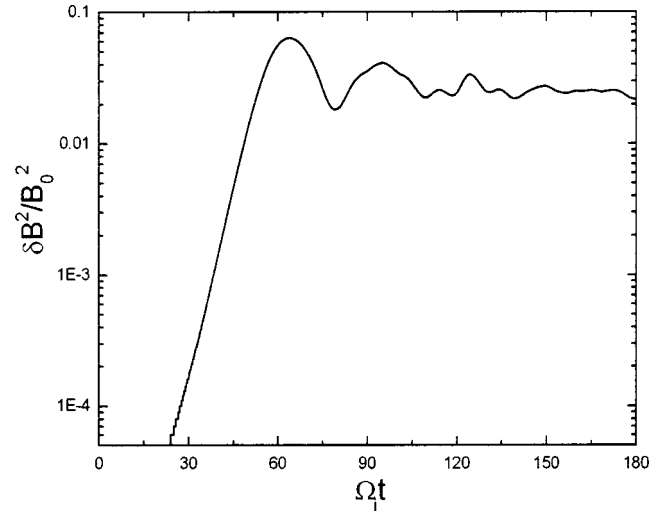

FIG. 5. The time evolutions of total magnetic field energy ε_B in logarithmic scale, the parameters are $n_b/n_0=0.006$ and $\beta_i=0.04$.

We have also simulated the cases $n_b/n_0=0.01$ and 0.05; the results are similar to the case $n_b/n_0=0.006$. The interaction between the background and tenuous beam plasma can excite right-hand side resonant waves, which can scatter the beam electron into a ring velocity distribution and heat the beam and background electrons.

IV. CONCLUSIONS

In summary, we have simulated the nonlinear beam–plasma interaction process with emphasis placed on the study of the velocity distribution of the beam electrons during the process. From the simulation results, we find the following salient points.

Because the density of the beam particles is tenuous, the resonant instability of the right-hand side mode is generally dominant, and the excited waves are low-frequency Alfvén waves. This is in agreement with previous investigations reported in literature. The time evolution of these waves consists primarily of four phases: The initial growth, saturation, postsaturation and quasi-equilibrium phases, which are consistent with the results obtained by Wang and Lin with 1D and two-dimensional hybrid simulations, although they use a longer system length.[29]

However, our main interest is how these waves affect the velocity distribution of the beam electrons. With PIC simulations, we are able to study this issue. The details have already been discussed in Sec. III. Here, we only summarize

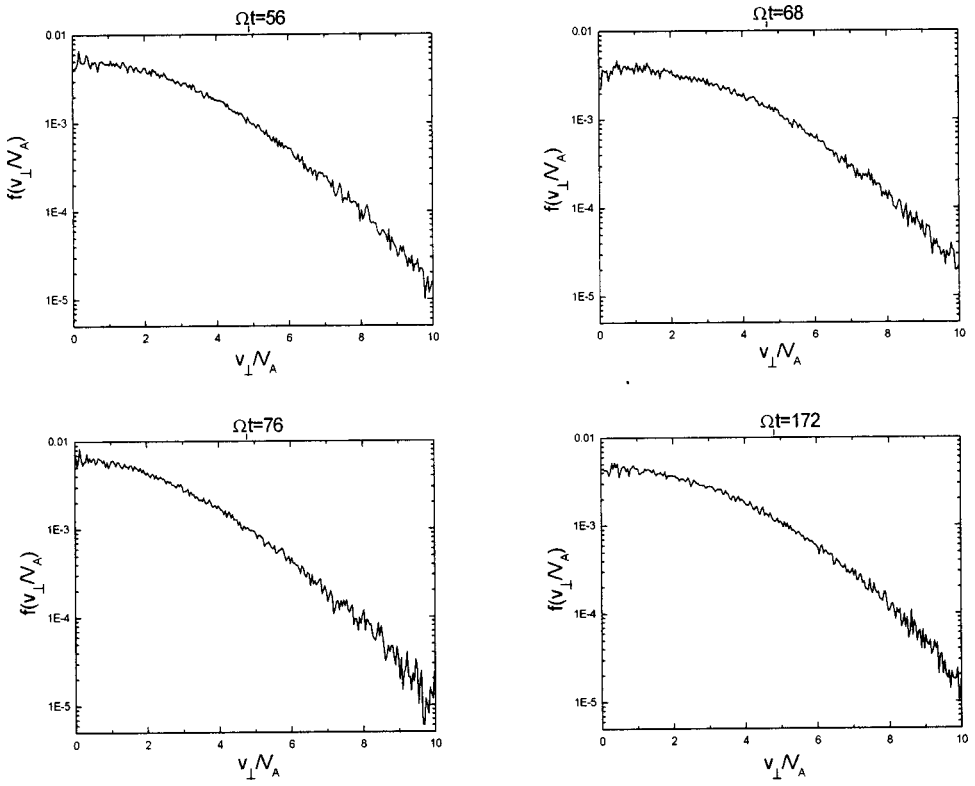

FIG. 6. The reduced velocity distribution in the direction perpendicular to the ambient magnetic field $f(u_\perp)$ at different times $t=56\,\Omega_i^{-1}$, $68\,\Omega_i^{-1}$, $76\,\Omega_i^{-1}$ and $172\,\Omega_i^{-1}$, the parameters are $n_b/n_0=0.006$ and $\beta_i=0.04$.

the main conclusions. When β_i is sufficiently low (<0.01), in the linear growth phases, the perpendicular velocity distribution of the beam electrons can be pitch–angle scattered into a ring-like distribution, and, as a result, there exists a positive $\partial f(u_\perp)/\partial u_\perp$ region. The radius of the positive $\partial f(u_\perp)/\partial u_\perp$ region is correlated with the magnetic fluctuation level. It reaches a peak value at the saturation stage, and decreases at the postsaturation stage. At the quasi-equilibrium phase, the positive $\partial f(u_\perp)/\partial u_\perp$ region in the velocity distribution of the beam electrons still persists. But, the ring distribution disappears at the quasi-equilibrium phase if the ion beta is sufficiently high. For example, when

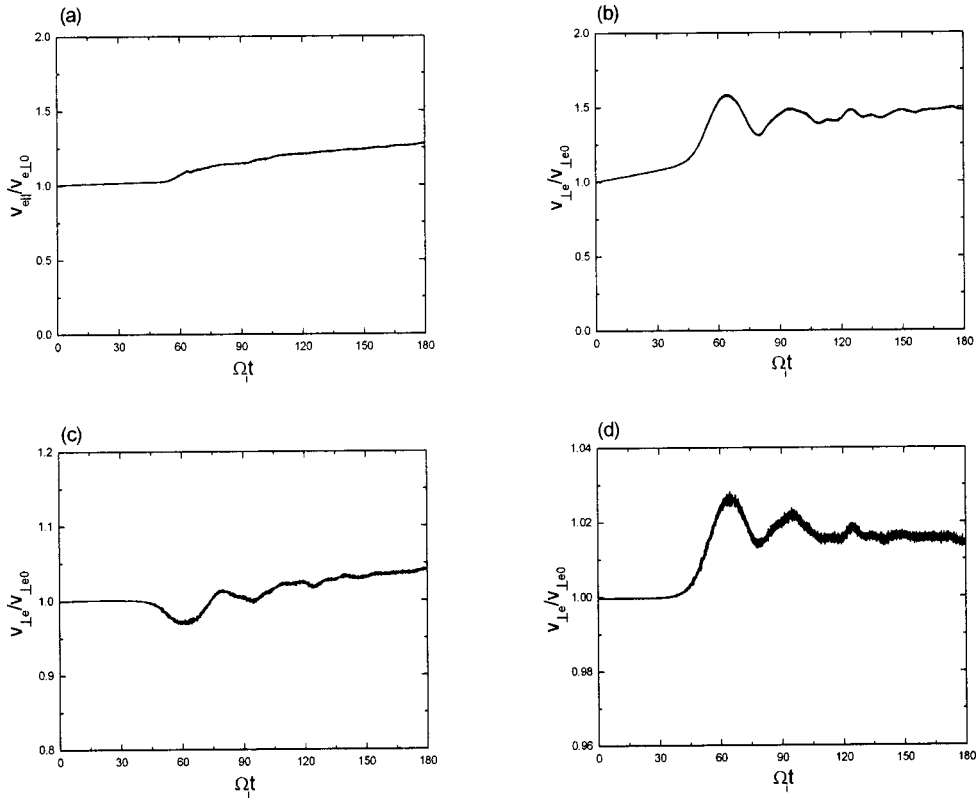

FIG. 7. The thermal speed of the beam and background electrons as a function of time, the parameters are $n_b/n_0=0.006$ and $\beta_i=0.04$. (a) The thermal speed of beam electrons in the direction parallel to the background magnetic field. (b) The thermal speed of beam electrons in the direction perpendicular to the background magnetic field. (c) The thermal speed of background electrons in the direction parallel to the background magnetic field. (d) The thermal speed of beam electrons in the direction perpendicular to the background magnetic field. $\nu_{\parallel e0}$ and $\nu_{\perp e0}$ denote the initial electron thermal speed in the direction parallel and perpendicular background magnetic field.

$\beta_i \geqslant 0.01$, and even at the saturation phase it disappears when $\beta_i \geqslant 0.2$.

Another interesting and significant point is that both the beam and background electrons can be heated by the excited Alfvén waves when the turbulence level is reasonably high. But their final thermal speeds are anticorrelated with the parameter β_i. When $\beta_i = 4 \times 10^{-4}$, the final thermal speeds of the beam electrons are about 10 and 6 times of their initial thermal speeds in the direction parallel and perpendicular to the background magnetic field, while the corresponding values are about 5.2 and 1.6 for the thermal speeds of the background electrons. However, in the higher beta case, the heating effects are much less obvious. For instance, as shown in Fig. 7, when $\beta_i = 0.04$, the increase of the thermal speeds of the beam electrons is about 1.25 and 1.50 in the direction parallel and perpendicular to the background magnetic field, while the heating of the background electrons is negligible. In short, the heating effect is more significant for the beam electrons than the background electrons. Heating in the parallel direction seems to be attributed to the direct nonlinear interaction with the excited waves, whereas it appears that, in the very low beta case, pitch–angle scattering plays an initial role in the heating in the perpendicular direction. Pitch–angle scattering can first result in the formation of a ringlike distribution and, subsequently, the enhanced waves randomize the beam distribution to broaden the velocity dispersion.

ACKNOWLEDGMENTS

This research was supported by the National Science Foundation of China (NSFC) under Grant Nos. 40084001, 40174041, and 40244006 and the Chinese Academy of Sciences Grant No. KJCX2-N08.

[1] C. T. Russell, Planet. Space Sci. **20**, 1541 (1972).
[2] K. Takahashi and E. W. Hones, J. Geophys. Res. **93**, 8558 (1988).
[3] D. Winske, C. S. Wu, Y. Y. Li, Z. Z. Mou, and S. Y. Guo, J. Geophys. Res. **90**, 2813 (1985).
[4] M. Scholer and D. Burgess, J. Geophys. Res. **97**, 8319 (1992).
[5] N. Dubouloz and M. Scholer, J. Geophys. Res. **100**, 9461 (1995).
[6] W. C. Feldman, J. R. Asbridge, S. J. Bame, and M. D. Montgery, J. Geophys. Res. **79**, 2773 (1974).
[7] E. Marsh, K. H. Muhlhauser, R. Schwenn, H. Rosenbauer, W. Pilipp, and F. M. Naubauer, J. Geophys. Res. **87**, 52 (1982).
[8] W. Daughton, S. P. Gary, and D. Winske, J. Geophys. Res. **104**, 4657 (1999).
[9] T. E. Hozer and W. I. Axford, J. Geophys. Res. **76**, 6965 (1971).
[10] C. S. Wu, R. E. Hartle, and K. Ogilvie, J. Geophys. Res. **78**, 306 (1973).
[11] R. E. Hartle and C. S. Wu, J. Geophys. Res. **78**, 5802 (1973).
[12] W. C. Feldman, J. T. Gosling, D. J. McComas, and J. L. Phillips, Astron. Astrophys. **316**, 5593 (1996).
[13] Y. P. Chen, G. C. Zhou, and C. S. Wu, Sol. Phys. (to be published).
[14] C. S. Wu and R. C. Davidson, J. Geophys. Res. **77**, 5399 (1972).
[15] C. S. Wu and R. E. Hartle, J. Geophys. Res. **79**, 293 (1974).
[16] C. S. Wu, D. Winske, and J. D. Gaffey, Geophys. Res. Lett. **13**, 865 (1986).
[17] B. T. Tsurutani and E. J. Smith, Geophys. Res. Lett. **13**, 263 (1986).
[18] P. H. Yoon and C. S. Wu, in *Cometary Plasma Processes*, edited by A. D. Johnstone (American Geophysical Union, Washington, DC, 1991), p. 241.
[19] Y. Li, P. H. Yoon, C. S. Wu, A. T. Weatherwax, J. K. Chao, and B. H. Wu, Phys. Plasmas **4**, 4103 (1997).
[20] C. S. Wu, P. Y. Yoon, and J. K. Chao, Phys. Plasmas **4**, 856 (1997).
[21] L. Chen, Z. Lin, and R. White, Phys. Plasmas **8**, 4713 (2001).
[22] C. K. Birdsall and A. B. Langdon, *Plasma Physics via Computer Simulation*, Adam Hilger Series on Plasma Physics (Hilger, New York, 1991).
[23] Q. M. Lu and D. S. Cai, Comput. Phys. Commun. **135**, 93 (2001).
[24] T. Terasawa, M. Hoshino, J. I. Sakai, and T. Hada, J. Geophys. Res. **91**, 4171 (1986).
[25] R. H. Miller, T. I. Gombosi, S. P. Gary, and D. Winske, J. Geophys. Res. **96**, 9749 (1991).
[26] K. Akimoto, J. Geophys. Res. **96**, 17599 (1991).
[27] K. Akimoto, D. Winske, S. P. Gary, and M. F. Thomsen, J. Geophys. Res. **98**, 1419 (1993).
[28] C. S. Wu, C. B. Wang, P. H. Yoon, H. N. Zheng, and S. Wang, Astrophys. J. **575**, 1049 (2002).
[29] X. Y. Wang and Y. Lin, Phys. Plasmas **10**, 3528 (2003).